JOURNAL OF APPLIED PHYSICS **116**, 124514 (2014)

Improvement of resistive switching performances via an amorphous ZrO_2 layer formation in TiO_2-based forming-free resistive random access memory

Baiwen Zeng, Dinglin Xu, Minghua Tang,[a] Yongguang Xiao, Yuzhou Zhou, Rongxin Xiong, Zheng Li,[b] and Yichun Zhou
The Key Laboratory of Low Dimensional Materials and Application Technology of Ministry of Education, Xiangtan University, Xiangtan, Hunan 411105, China

(Received 5 June 2014; accepted 13 September 2014; published online 29 September 2014)

We present the effects of an amorphous ZrO_2 layer on the TiO_2-based bipolar resistive switching memory device where the ZrO_2 layer plays an important role as a supplementary reservoir of oxygen vacancies. Compared with Pt/TiO_2/Pt monolayer device, a remarkably improved uniformity of switching parameters such as switching voltages and resistances in high/low states is demonstrated in the Pt/ZrO_2/TiO_2/Pt system. The resistive switching mechanism of memory devices incorporating the ZrO_2/TiO_2 bilayer structure can be attributed to multiple conducting filaments through the occurrence of redox reactions at the ZrO_2/TiO_2 surface. © *2014 AIP Publishing LLC.*
[http://dx.doi.org/10.1063/1.4896402]

As one of the most promising candidates for next-generation nonvolatile memory, resistive random access memory (RRAM) has attracted great attention due to its potential advantages of simple structure, high speed operation, low power consumption, long retention time, nondestructive readout, and good compatibility with complementary metal oxide semiconductor (CMOS) technology.[1] Various polycrystalline and amorphous transition metal oxides (TMOs), including ZrO_2, TiO_2, ZnO, and HfO_2, have found their applications in RRAMs.[2–5]

Excellent resistive switching (RS) performances such as large resistance ratio, good retention, and endurance properties have been demonstrated in TiO_2-based RRAM devices.[6] However, finding an effective way to improve the stabilization of RS performance is still a challenge. Up to now, various research approaches, such as doping[7] and preparation of composite structures,[8] have been proposed to improve the RS performances of TiO_2-based RRAM devices.

In this study, by embedding an amorphous ZrO_2 layer to fabricate a Pt/ZrO_2/TiO_2/Pt structure device, we found that the Pt/ZrO_2/TiO_2/Pt device possesses excellent bipolar RS performances in comparison with Pt/TiO_2/Pt device, including low switching voltage, narrow switching voltage distribution, and good cycling endurance.

The ZrO_2/TiO_2 bilayer structure was prepared on Pt(111)/Ti/SiO_2/Si substrate using the sol-gel method. The precursor titanium isopropoxide (TIPP) was then peptized in ethanol at a concentration of 0.4 M. Next, a stable TiO_2 solution was prepared by mixing this precursor with nitric acid and deionized water in a molar ratio of 1:0.82:0.13. The ZrO_2 solution was prepared separately by dispersing zirconium oxychloride octahydrate in ethanol at a concentration of 0.4 M. To fabricate the ZrO_2/TiO_2 bilayer structure, three layers of TiO_2 and one layer of ZrO_2 were spin-coated on the substrate at a speed of 3000 rpm for 30 s. Each layer of TiO_2 was dried at 150 °C for 5 min and finally annealed at 400 °C for 1 h in air atmosphere. The ZrO_2 layer was deposited subsequently on the TiO_2 film under the same process (400 °C for 1 h). The synthesized films were examined by X-ray diffraction (XRD), scanning electron microscopy (SEM), and X-ray photoelectron spectroscopy (XPS) analysis. To achieve sandwich-structure devices, a top Pt electrode (TE) with a diameter of 200 μm was deposited by magnetron sputtering with a metal shadow mask, the thickness of the TE was around 200 nm. Electrical measurements of fabricated device were performed using a Keithley 4200-SCS semiconductor parameter analyzer.

Fig. 1(a) shows the XRD θ-2θ scan results of the ZrO_2/TiO_2 thin films grown on Pt substrates, and it illustrates that the main crystalline phase of the TiO_2 layer is rutile. It is worth noting that there is no significant discrepancy between the XRD patterns of the TiO_2-based devices with or without the growth of the ZrO_2 layer. Then, the crystallinity and phase of ZrO_2 layer are investigated by using grazing incidence XRD (GIXRD). As shown in Fig. 1(b), no characteristic peak could be observed in the GIXRD pattern of ZrO_2 film grown on Pt substrate. It is suggested here that the solution-based deposition of the ZrO_2 film produces an amorphous phase while the TiO_2 film is polycrystalline. Furthermore, the thicknesses of the TiO_2 layer and ZrO_2 layer obtained are about 150 nm and 50 nm from the cross section graph of SEM, respectively, as shown in the inset of Fig. 1(a).

In order to clarify the chemical composition of ZrO_2/TiO_2 bilayer film, XPS spectra related to the ZrO_2 layer and TiO_2 layer were carried out, respectively, as shown in Fig. 2. The peaks corresponding to ZrO_2 with peak binding energies of 182.2 eV (Zr $3d_{5/2}$) and 184.5 eV (Zr $3d_{3/2}$) are observed in the XPS spectra of ZrO_2 layer (Fig. 2(a)), which confirm the formation of zirconium dioxide. Fig. 2(b) illustrates that the oxidation state of titanium is Ti^{4+}. The Ti $2p_{3/2}$ and Ti $2p_{1/2}$ peaks are observed at binding energies of

[a]Electronic mail: mhtang@xtu.edu.cn. Tel.: +86-731-58292200. Fax: +86-731-58292468.
[b]Electronic mail: lizheng@xtu.edu.cn. Tel.: +86-731-58292200. Fax: +86-731-58292468.

 © 2014 AIP Publishing LLC

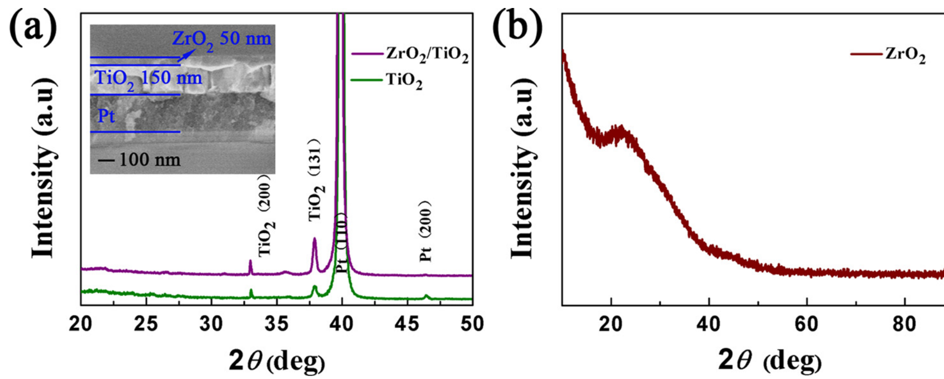

FIG. 1. (a) XRD θ-2θ scan results of the ZrO_2/TiO_2 film grown on Pt/Ti/SiO_2/Si substrates, the inset shows the thickness of the ZrO_2/TiO_2 thin film. (b) GIXRD pattern of the ZrO_2 film.

around 458.8 eV and 464.5 eV, respectively, which are very close to those observed in the case of bulk TiO_2.[9] Additionally, as shown in Fig. 2(c), both XPS spectra at the O 1 s-edge of TiO_2 layer and ZrO_2 layer can be deconvoluted into two peaks corresponding to O-Ti and non-lattice oxygen.[9–11] In contrast to the TiO_2 layer, a higher proportion of non-lattice oxygen exists in the ZrO_2 layer, which reveals that more oxygen vacancies and structural defects exist in the amorphous ZrO_2 layer.[12]

Figs. 3(a) and 3(b) show typical *I-V* characteristics of the Pt/TiO_2/Pt and Pt/ZrO_2/TiO_2/Pt devices, respectively. Once a positive bias was applied, both Pt/TiO_2/Pt and Pt/ZrO_2/TiO_2/Pt devices switch from high resistivity state (HRS) to low resistivity state (LRS), which is called a "set" process. Furthermore, a change of resistance from LRS to HRS, namely, a "reset" process, could be achieved by a negative bias sweep. Here, a current compliance of 0.01 A was imposed during the set process to prevent irreversible dielectric damage. It is well known that most pristine oxides require an additional ''electro-forming'' process prior to the repetitive dc sweep. This process involves the initial application of a high electric field to locally generate conductive filaments across the dielectric via a soft breakdown.[13] However, the forming process was required in neither the Pt/TiO_2/Pt device nor the Pt/ZrO_2/TiO_2/Pt device, as shown in Figs. 3(a) and 3(b). It is most likely that the abundance of initial amount of oxygen vacancies produce the observed forming-free characteristics of the samples.[14] In addition, the Pt/ZrO_2/TiO_2/Pt device exhibits a lower switching voltage and a more stable RS performance. The distribution of switching voltages in the Pt/ZrO_2/TiO_2/Pt device is obviously narrower than that in the Pt/TiO_2/Pt device. The phenomenon is further quantified in histograms of V_{set} and V_{reset} for both types of devices (Fig. 3(c)).

As shown in Fig. 3(c), the dispersion of V_{set} and V_{reset} for the Pt/ZrO_2/TiO_2/Pt device is reduced in comparison with the TiO_2 monolayer structure device. The average values of V_{set} and V_{reset} of the Pt/ZrO_2/TiO_2/Pt device are about 2.34 and −0.6 V, respectively, which are lower than those of Pt/TiO_2/Pt (2.62 and −0.95 V). The reduced switching voltage of the Pt/ZrO_2/TiO_2/Pt device is most likely due to the supplement of oxygen vacancies from the amorphous ZrO_2 layer to the TiO_2 layer for the recovery/rupture of metallic paths inside the TiO_2.[15] Furthermore, the endurance test of 200 cycles for Pt/ZrO_2/TiO_2/Pt bilayer devices provides evidence of more stable performance, as shown in Fig. 3(d). After 50-cycle tests, resistances of ∼50 Ω and∼130 kΩ at LRS and HRS with a read voltage of 0.5 V can be observed in the Pt/ZrO_2/TiO_2/Pt device, yielding a stable R_{HRS}/R_{LRS} ratio of ∼2600. Recently, a similar improvement of the uniformity of switching parameters was also reported for Lee's ZrO_x/HfO_x bilayer structure device.[16] Lee claimed that in the case of the monolayer structure, the active filament participating in the switching process is controlled by competition among parallel conductive filaments; however, the resistive switching of the bilayer structure is induced by a redox reaction at the tip of the local filament in the ZrO_2/TiO_2 interface.[16] During the switching process, the amorphous ZrO_2 layer plays an important role as a supplementary reservoir of oxygen vacancies. Hence, by using the bilayer structure, a remarkably improved uniformity of switching parameters can be achieved.

To further understand the resistive switching characteristics, the classical nonlinear conduction mechanisms, including Poole-Frenkel (PF) emission,[17] Schottky-like emission,[18] and space charge limited current (SCLC),[19] were adopted to fit the nonlinearity of the measured *I-V* relation. The plot of Log*I*-Log*V* of the Pt/ZrO_2/TiO_2/Pt device is

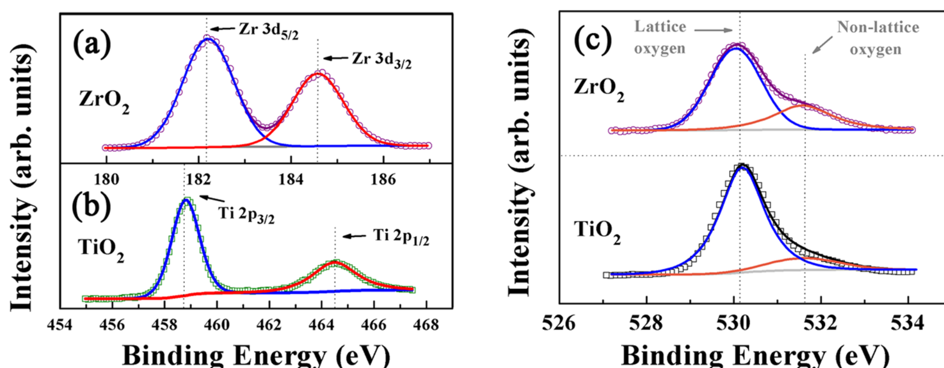

FIG. 2. XPS spectra of (a) Zr 3d in the ZrO_2 layer, (b) Ti 2p in the TiO_2 layer. (c) Comparison of XPS spectra of O 1s in the ZrO_2 and TiO_2 layers.

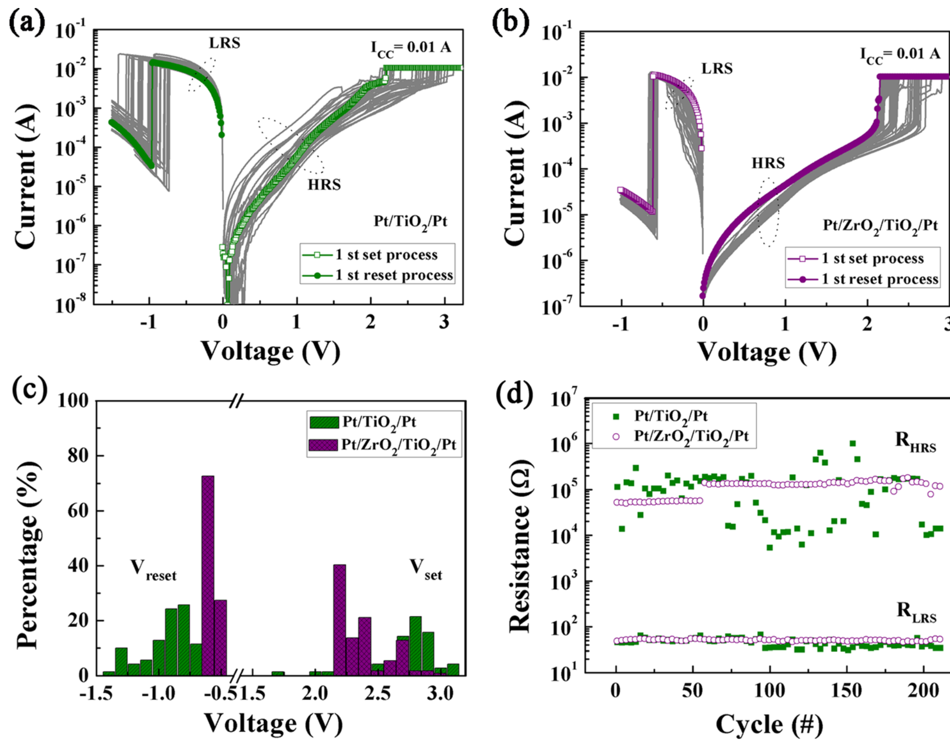

FIG. 3. Memory switching I-V curves in the (a) Pt/TiO_2/Pt and (b) Pt/ZrO_2/TiO_2/Pt memory cells. The data are from continuous memory switchings of 100 times. (c) Histograms of operation voltage and (d) distribution of both states' resistance in Pt/TiO_2/Pt and Pt/ZrO_2/TiO_2/Pt devices.

shown in Fig. 4. The conduction behavior in the LRS is Ohmic because the curve of the Log$I$-Log$V$ is a linear line with a slope of about 1. However, the current in the HRS is governed by the trap-controlled SCLC model.[19] The I-V curve of the HRS can be divided into two parts as represented by the different slopes of the linear fitting. At the low voltage region, the injected carrier density is lower than the thermally generated carrier density and the conduction follows Ohm's law ($I \sim V$). With increasing V, the injected carriers become predominant. When all of the traps are filled with the injected carriers under the higher voltage, a sudden jump in current occurs at around 0.6 V and then the I-V behavior follows Child's law ($I \sim V^2$). Eventually, the sample switches to the LRS at V_{set}. Consequently, The HRS's conduction characteristic is in agreement with the trap-controlled SCLC.

The possible migration of oxygen vacancies from the amorphous ZrO_2 layer to the TiO_2 layer is schematically illustrated in Fig. 5. The possibility of RS behavior of the bilayer structure device is based on oxygen vacancies migration-induced oxidation/reduction reaction at the interface of ZrO_2/TiO_2. Kwon *et al*. reported that RS in polycrystalline TiO_2 film was caused by the formation and disruption of suboxide phase (Magnéli phase) filaments, and that the conductive filaments had a conical shape, where the conductive filaments at the anode side has a smaller diameter than that at the cathode side.[20] Once positive bias is applied to the uppermost Pt electrode, as shown in Fig. 5(a), oxygen vacancies ejected from the amorphous ZrO_2 layer migrate toward the TiO_2 layer. With this increase in concentration of oxygen vacancies in the TiO_2 layer, there should be a strong thermodynamic driving force to form the Magnéli phase conducting filaments.[20] As a result, the device goes to LRS. In the reset operation as shown in Fig. 5(b), the repealed oxygen ions from the ZrO_2 layer together cause local oxidization at the tip of the localized filament.[13,20] Consequently, the connected Magnéli phase filaments should be ruptured bringing the device into HRS. Thus, the ZrO_2 layer works like oxygen reservoir, storing, and releasing the oxygen during switching operation.

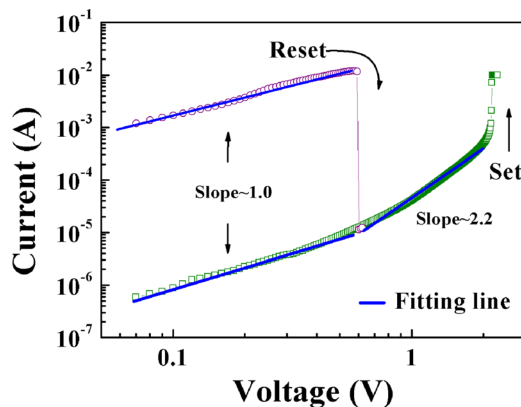

FIG. 4. The Log-Log plot I-V of the HRS and LRS of the Pt/ZrO_2/TiO_2/Pt device. The blue lines show the fitting.

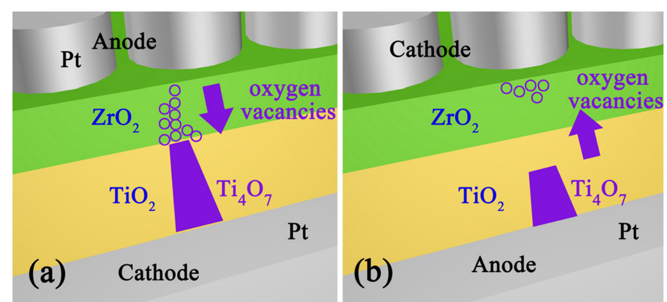

FIG. 5. Schematic of ZrO_2/TiO_2 bilayer structure under (a) positive bias and (b) negative bias.

We have investigated the bipolar RS behavior of TiO_2-based RRAM device by embedding an amorphous ZrO_2 layer between Pt TE and TiO_2. The RS characteristics of the $Pt/ZrO_2/TiO_2/Pt$ bilayer structure device are greatly improved as compared to those of the $Pt/TiO_2/Pt$ device, such as lower power consumption and the improved uniformity of switching parameters such as switching voltages and resistances in high/low states. The improvement of the RS characteristics can be attributed to the amorphous ZrO_2 layer which modifies the oxygen vacancies in the TiO_2 layer.

This work was financially supported by Key Project of National Natural Science Foundation of China (NSFC) (Grant No. 11032010), NSFC (Grant No. 61274107), 973 Program (Grant No. 2012CB326404), and Key Project of Hunan Provincial NSFC (Grant No. 13JJ2023).

[1]G. I. Meijer, Science **319**, 1625 (2008).
[2]Q. Liu, S. Long, W. Wang, Q. Zuo, S. Zhang, J. Chen, and M. Liu, IEEE Electron Device Lett. **30**, 1335 (2009).
[3]M. H. Tang, B. Jiang, Y. G. Xiao, Z. Q. Zeng, Z. P. Wang, J. C. Li, and J. He, Microelectronic Eng. **93**, 35 (2012).
[4]B. Sun, Y. X. Liu, L. F. Liu, N. Xu, Y. Wang, X. Y. Liu, R. Q. Han, and J. F. Kang, J. Appl. Phys. **105**, 061630 (2009).
[5]H. Y. Lee, Y. S. Chen, P. S. Chen, T. Y. Wu, F. Chen, C. C. Wang, P. J. Tzeng, M.-J. Tsai, and C. Lien, IEEE Electron Device Lett. **31**, 44 (2010).
[6]C. Lee, I. Kim, W. Choi, H. Shin, and J. Cho, Langmuir **25**, 4274 (2009).
[7]L. F. Liu, Y. S. Chen, J. F. Kang, Y. Wang, D. D. Han, X. Y. Liu, and X. Zhang, Semicond. Sci. Technol. **26**, 115009 (2011).
[8]H. B. Zhao, H. L. Tu, F. Wei, X. Q. Zhang, Y. H. Xiong, and J. Du, Solid-State Electron. **89**, 12 (2013).
[9]K. P. Biju, X. J. Liu, E. M. Bourim, I. Kim, S. Jung, M. Siddik, J. Lee, and H. Hwang, J. Phys. D: Appl. Phys. **43**, 495104 (2010).
[10]C.-C. Lin, Y.-P. Chang, H.-B. Lin, and C.-H. Lin, Nanoscale Res. Lett. **7**, 187 (2012).
[11]J. Shin, I. Kim, K. P. Biju, M. Jo, J. Park, J. Lee, S. Jung, W. Lee, S. Kim, S. Park, and H. Hwang, J. Appl. Phys. **109**, 033712 (2011).
[12]T. Szörényi, L. D. Laude, I. Bertóti, Z. Kántor, and Z. Geretovszky, J. Appl. Phys. **78**, 6211 (1995).
[13]K. M. Kim, D. S. Jeong, and C. S. Hwang, Nanotechnology **22**, 254002 (2011).
[14]M. S. Lee, S. Choi, C.-H. An, and H. Kim, Appl. Phys. Lett. **100**, 143504 (2012).
[15]C.-H. Huang, J.-S. Huang, S.-M. Lin, W.-Y. Chang, J.-H. He, and Y.-L. Chueh, ACS Nano **6**, 8407 (2012).
[16]J. Lee, E. M. Bourim, W. Lee, J. Park, M. Jo, S. Jung, J. Shin, and H. Hwang, Appl. Phys. Lett. **97**, 172105 (2010).
[17]J. R. Yeargan and H. L. Taylor, J. Appl. Phys. **39**, 5600 (1968).
[18]P. R. Emtage and W. Tantraporn, Phys. Rev. Lett. **8**, 267 (1962).
[19]M. A. Lampert and P. Mark, *Current Injection in Solids* (Academic, New York, 1970).
[20]D.-H. Kwon, K. M. Kim, J. H. Jang, J. M. Jeon, M. H. Lee, G. H. Kim, X.-S. Li, G.-S. Park, B. Lee, S. Han, M. Kim, and C. S. Hwang, Nat. Nanotechnol. **5**, 148 (2010).

Journal of Applied Physics is copyrighted by the American Institute of Physics (AIP). Redistribution of journal material is subject to the AIP online journal license and/or AIP copyright. For more information, see http://ojps.aip.org/japo/japcr/jsp